ADVANCES IN ATMOSPHERIC SCIENCES, VOL. 32, MAY 2015, 680–689

Seasonal Prediction of June Rainfall over South China: Model Assessment and Statistical Downscaling

Kun-Hui YE[†1], Chi-Yung TAM[*‡1,2], Wen ZHOU[1,2], and Soo-Jin SOHN[3]

[1]*Guy Carpenter Asia-Pacific Climate Impact Centre, City University of Hong Kong, Hong Kong, China*
[2]*School of Energy and Environment, City University of Hong Kong, Hong Kong, China*
[3]*Climate Prediction Team, APEC Climate Center, Busan, Republic of Korea*

(Received 18 March 2014; revised 8 September 2014; accepted 8 October 2014)

ABSTRACT

The performances of various dynamical models from the Asia-Pacific Economic Cooperation (APEC) Climate Center (APCC) multi-model ensemble (MME) in predicting station-scale rainfall in South China (SC) in June were evaluated. It was found that the MME mean of model hindcasts can skillfully predict the June rainfall anomaly averaged over the SC domain. This could be related to the MME's ability in capturing the observed linkages between SC rainfall and atmospheric large-scale circulation anomalies in the Indo-Pacific region. Further assessment of station-scale June rainfall prediction based on direct model output (DMO) over 97 stations in SC revealed that the MME mean outperforms each individual model. However, poor prediction abilities in some in-land and southeastern SC stations are apparent in the MME mean and in a number of models. In order to improve the performance at those stations with poor DMO prediction skill, a station-based statistical downscaling scheme was constructed and applied to the individual and MME mean hindcast runs. For several models, this scheme can outperform DMO at more than 30 stations, because it can tap into the abilities of the models in capturing the anomalous Indo-Pacific circulation to which SC rainfall is considerably sensitive. Therefore, enhanced rainfall prediction abilities in these models should make them more useful for disaster preparedness and mitigation purposes.

Key words: June South China rainfall, multi-model ensemble prediction, statistical downscaling, bias correction

Citation: Ye, K.-H., C.-Y. Tam, W. Zhou, and S.-J. Sohn, 2015: Seasonal prediction of June rainfall over South China: Model assessment and statistical downscaling. *Adv. Atmos. Sci.*, **32**(5), 680–689, doi: 10.1007/s00376-014-4047-x.

1. Introduction

Over South China (SC), the June monthly mean rainfall and its interannual variability are the largest in magnitude among those throughout the calendar year (Yuan et al., 2012). In fact, the outbreak of the South China Sea summer monsoon (SCSSM) occurs climatologically in the fourth pentad of May (Murakami and Matsumoto, 1994; Wu and Wang, 2000; Gao et al., 2001; Zhou et al., 2005), and its associated rainband migrates northward in mid-to-late June. After the SCSSM onset, precipitation over SC increases dramatically, marking the beginning of the seasonal march of the summer monsoon rainband (Ding, 2004). Accurate seasonal forecasts of the June SC rainfall would be invaluable for the water management sector, as well as for mitigation and disaster preparedness in the region.

On the interannual timescale, there are a number of circulation systems that can greatly influence the SC summertime rainfall. The western North Pacific subtropical high (WNPSH), in particular, can strongly influence the SC summer rainfall through its east–west displacement and strength (Chang et al., 2000; Yang and Sun, 2005). In fact, SST anomalies in both the South China Sea (SCS) (Zhou and Chan, 2007) and the Indian Ocean (Yuan et al., 2008; Xie et al., 2009) are able to affect SC through such a link between the WNPSH and SC rainfall. An out-of-phase relationship between the rainfall of regions surrounding the SCS and Indian summer monsoon (ISM) rainfall has also been proposed (Kripalani and Kulkarni, 2001). In addition, extratropical atmospheric activities can affect SC rainfall. Zhang and Tao (1998) pointed out that the persistent blocking high over the Sea of Okhotsk could give rise to above-normal precipitation in summer over East Asia. Also, the arrival of midlatitude fronts may be linked to the onset of the SCSSM (Chang and Chen, 1995; Tong et al., 2009). Yuan et al. (2012) concluded that extratropical forcing induced by the west Siberian low was an important contributor to the excessive June rainfall in 2010 over SC. Finally, equatorial eastern Pacific SST is a prominent climatic factor that influences the SC rainfall.

† Current address: Institute of Space and Earth Information Science, the Chinese University of Hong Kong, Hong Kong
* Corresponding author: Chi-Yung TAM
Email: Francis.Tam@cuhk.edu.hk
‡ Current address: Earth System Science Programme, The Chinese University of Hong Kong, Shatin, N.T., Hong Kong

For example, SC may suffer from droughts in the developing stage of ENSO, whereas floods are likely to occur over SC when the latter decays (Huang and Wu, 1989). Chang et al. (2000) found that summer rainfall during the period 1951–77 was stronger than that during the period 1978–96 in the southeastern coastal area of China, due to a stronger and more expansive mean western Pacific subtropical ridge caused by higher mean equatorial eastern Pacific SST over the course of the latter period.

General circulation models (GCMs) are widely used for seasonal forecasting, but still lack sufficient ability in reproducing climate at the local scale (Stockdale et al., 1998). In the Asian summer monsoon region, for instance, state-of-the-art coupled models generally have difficulties in capturing the mean precipitation, even with a one-month lead time (Wang et al., 2007, 2008, 2009; Kug et al., 2008; Lee et al., 2010). Nevertheless, in terms of predicting the East Asian and western North Pacific monsoon, models tend to perform better when forecasting after the mature phase of ENSO (Wang et al., 2009; Liang et al., 2009; Chowdary et al., 2010; Lee et al., 2011a; Lee et al., 2011b). In recent years, the multi-model ensemble (MME) method (Krishnamurti et al., 1999, 2000; Doblas-Reyes et al., 2000) has been adopted by several major operational centers for seasonal climate prediction (Palmer et al., 2004; Lee et al., 2009). In the present reported study, we used the hindcast runs from various climate models participating in the Asia-Pacific Economic Cooperation (APEC) Climate Center (APCC) MME to assess their performance in predicting SC rainfall. In addition, we established a station-based statistical downscaling scheme for the SC region in an attempt to enhance the rainfall prediction abilities of some of the models. Statistical downscaling, the fundamental principle of which is to derive local climate anomalies from the large-scale circulation, is widely regarded as a technique that can improve model predictions (e.g., Karl et al., 1990; Wigley et al., 1990; Wilby and Wigley, 1997; Kang et al., 2007; Sohn et al., 2013a). Indeed, a pattern-based statistical downscaling approach for SC summer rainfall prediction has previously been tested by Tung et al. (2013). Liu et al. (2011) also used statistical downscaling for summer rainfall prediction, but in a smaller domain in the eastern part of SC. Several other studies have also attempted to improve model prediction by statistical methods (Wang and Fan, 2009; Fan et al., 2008, 2012; Liu and Fan, 2014).

The remainder of the paper is organized as follows: Section 2 provides a description of the models, datasets, and the statistical downscaling method. The results of the relationship between June rainfall and the large-scale circulation, the models' abilities to reproduce the June SC rainfall, and the performance of the downscaling prediction are presented in section 3. Finally, a brief discussion and summary of the key findings is provided in section 4.

2. Data and methods

2.1. *Observations and model hindcast data*

This study used the daily mean precipitation records from 740 stations over the SC region (18°–27°N, 105°–120°E). The geographical location of SC within China is shown in Fig. 1c. Inspection of the observational data revealed that, during the 1983–2003 period, 97 stations gave complete records of daily rainfall in June. Precipitation values from these 97 stations were considered in our analysis. The spatial distribution of these 97 stations is shown in Fig. 1d. In addition, 500 hPa geopotential height (Z500), 850 hPa wind, and the mean sea level pressure (SLP) from the National Centers for Environmental Prediction–Department of Energy (NCEP–DOE) Atmospheric Model Intercomparison Project (AMIP-II) reanalysis (Kanamitsu et al., 2002) were also used.

The APCC MME hindcast considered in this study comprises the seasonal prediction experiments from 11 climate models. They are provided by various operational centers and research institutes from the APEC economies including Canada, China, Korea, Taiwan, and the United States. Experiments of both the Seasonal Model Intercomparison Project/Historical Forecast Project (SMIP/HFP) and the Coupled Model Intercomparison Project (CMIP) types are involved, with the common hindcast period of 1983 to 2003. Table 1 provides details of these model experiments. All model predictions targeted in June were initiated in May of the same year, and the simulation results were interpolated onto the same $2.5^\circ \times 2.5^\circ$ grid. In addition to outputs from individual models, their MME average (which is the simple average of their products) was also considered in this study. In order to compare with observations, the models' rainfall outputs were spatially interpolated using bilinear interpolation onto the station locations in SC. Finally, as this study focuses on the interannual variability of the SC rainfall, long-term trends in both the observational and model data were removed prior to the analysis.

2.2. *Station-based statistical downscaling*

Besides using model precipitation to predict the SC rainfall, a statistical downscaling method with model SLP and Z500 values as predictors was also tested for predicting the June rainfall at station locations. The construction of the statistical prediction scheme is outlined as follows. First, correlation maps between station rainfall and SLP, as well as those with Z500, for each individual station location were inspected, in order to unveil any linkages between the Indo-Pacific large-scale circulation and SC rainfall. Results indicated that there were robust connections between rainfall variations observed at individual stations and SLP or Z500 signals from models over the ISM and western north Pacific regions (see also section 3.1). Adopting the model output statistics (MOS; Wilks, 1995) approach, model Z500 and SLP were then chosen as predictors for the observed station rainfall, based on the following equation:

$$P_i = a_i \mathrm{SLPA_A} + b_i \mathrm{Z500A_B} \ ,$$

where P_i is the June rainfall anomaly at station i, $\mathrm{SLPA_A}$ and $\mathrm{Z500A_B}$ represent the anomalous SLP and Z500 averaged over rectangular domains A and B located in the ISM

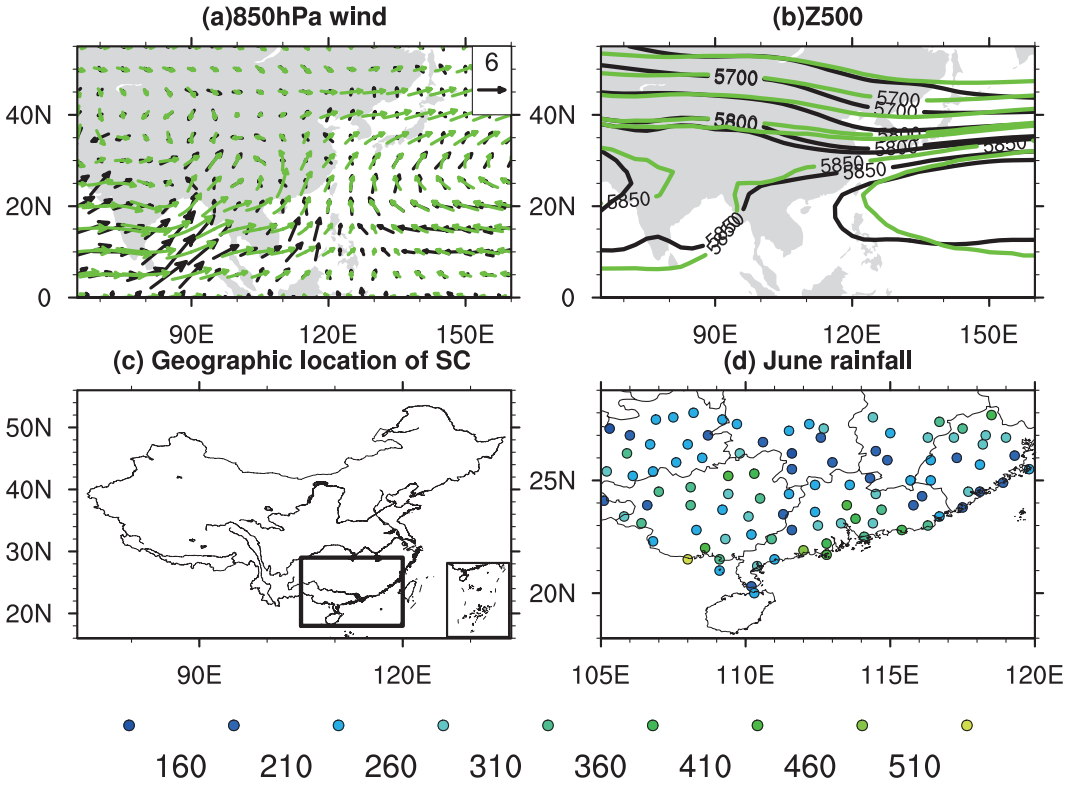

Fig. 1. Long-term mean (1983–2003) monthly (a) 850 hPa wind and (b) Z500 in June. Black (green) arrows and contours denote observed (MME average) 850 hPa wind and Z500 values, respectively. Units of scale arrows and contour lines for (a) and (b): m s^{-1} and gpm, respectively. (c) Geographical location of SC (denoted by the box). (d) Observed long-term mean accumulated rainfall in June at 97 station locations over SC (units: mm).

Table 1. Description of the hindcast experiments considered in this study.

Institute	Model	Resolution	Ensemble size	Experiment	Reference
Meteorological Service of Canada (MSC)	MSC-GM2	T32 L10	10	SMIP/HFP	McFarland et al. (1992)
MSC	MSC-GM3	T63 L32	10	SMIP/HFP	Scinocca et al. (2008)
MSC	MSC Spectral Primitive Eqt. Model (MSC-SEF)	T95 L27	10	SMIP/HFP	Ritchie (1991)
Korean Meteorological Administration (KMA)	Global Data Assimilation and Prediction system (GDAPS)	T106 L21	20	SMIP/HFP	Park et al. (2002)
National Institute of Meteorological Research (NIMR)	Meteorological Research Institute AGCM	$5^\circ \times 4^\circ$ L17	10	SMIP/HFP	Back et al. (2002)
Seoul National University (SNU)	Global Climate Prediction System (GCPS)	T63 L21	12	SMIP/HFP	Kang et al. (2004)
Central Weather Bureau (CWB)	CWB AGCM	T42 L18	10	SMIP/HFP	Liou et al. (1997)
Bureau of Meteorological Research Centre (BMRC)	Predictive Ocean-Atmosphere Model for Australia (POAMA)	T47 L17	10	CMIP	Zhong et al. (2005)
Beijing Climate Center (BCC)	BCC CGCM	T63 L16	8	CMIP	Ding et al. (2000)
National Centers for Environmental Prediction (NCEP)	NCEP Climate Forecast System (CFS)	T62 L64	15	CMIP	Saha et al. (2006)
Pusan National University (PNU)	PNU CGCM	T42 L18	5	CMIP	Sun and Ahn (2011)

region and western north Pacific, respectively. Note that the above represents an empirical relationship between station-scale rainfall and the large-scale circulation, and coefficients a_i and b_i (the values of which depend on the station being considered) are determined from model hindcast and station rainfall data by multiple linear regression. The exact location of domain A (B) can be found by first setting a "moving window" with 50° of longitude and 30° of latitude over the tropical Indian Ocean/Indian subcontinent (western north Pacific) area. The location of the window is then adjusted so that there are a maximum number of stations in SC with rainfall significantly correlated to the SLP (Z500) field over at least 1/3 of the grid points within domain A (domain B). Finally, the longitudinal and latitudinal extents of domains A and B are

fine-tuned, so as to capture the most number of stations in SC linked to either SLP or Z500 variations. Using this method, about 25% and 20% of the SC stations were identified with rainfall linked to SLP and Z500 variability over the Indo-Pacific, respectively. This scheme is processed at each station for every model, as well as for the MME average. For instance, domain A was found to be (20°N–10°S, 60°–110°E), while domain B covered (5°–25°N, 130°–180°E) when the MME mean SLP and Z500 were used. In this study, the statistical downscaling prediction was validated using a leave-one-out cross-validation framework. Such a framework seeks to mimic the actual forecast situation when data in the target period are not known; it is commonly used to validate predictions based on statistical schemes (e.g., Sohn et al., 2013b).

3. Results

3.1. *Relationship between SC rainfall and large-scale circulation*

Before analyzing the relationship between SC rainfall and large-scale circulation, the June climatological conditions from reanalysis data and model simulations were compared. Figures 1a and b show the reanalysis-based and MME mean values of Z500 and 850 hPa wind over Asia and the western Pacific in June. It can be seen that the MME 850 hPa wind circulation (green arrows in Fig. 1a) over the Indo-Pacific region compares well with reanalysis data (black arrows). Note that the position of the monsoon trough extending from northern Indochina into the SCS/Philippines Sea was also reproduced in the MME hindcasts. In addition, the WNPSH was also captured well by the MME hindcast (green contours in Fig. 1b), albeit with a slightly eastward shifted position compared with reanalysis data (black contours). The observed accumulated rainfall in June over SC is also shown (Fig. 1d). Overall, strong spatial variation is exhibited; monthly mean precipitation can reach the value of 500 mm in some southern coastal stations, while those over inland locations receive only 200 mm or less rainfall in the same month.

To examine how SC rainfall is related to the large-scale circulation over the Indo-Pacific region, Z500, SLP and the 850 hPa winds were regressed onto the precipitation averaged over SC in June. Figure 2 shows the regression coefficients computed based on observations as well as the MME average. From the reanalysis-based Z500 regression map, positive anomalies can be found centered over the Philippines to the SCS, and also in the western North Pacific (WNP) (Fig. 2a). Collocated with the former Z500 feature is an anomalous anticyclone in the lower levels (Fig. 2c). The above indicates a close relationship between SC precipitation variation and WNPSH activity. In particular, the low-level wind branch accompanying an anomalous high over the Philippines/WNP leads to stronger southerlies from the SCS. The latter is likely to transport more water vapor into SC, resulting in above-normal rainfall in the region. In addition to those in the subtropical western North Pacific, significant climate signals are also found in the northern Indian Ocean and at some extra-

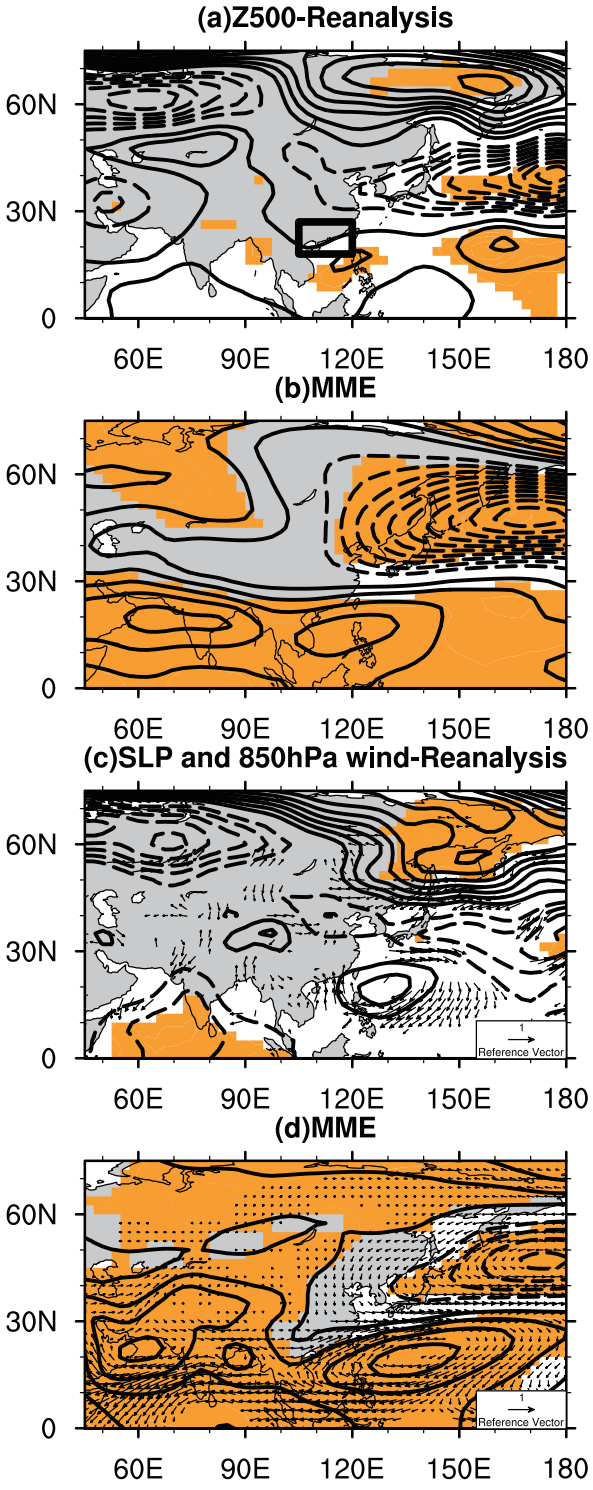

Fig. 2. Regression coefficients of the monthly mean (a, b) Z500, (c, d) SLP and 850 hPa wind based on the mean rainfall over SC in June for (a, c) reanalysis (but with observed rainfall) and (b, d) MME average. Dashed lines indicate negative values and shading (vectors) denote statistically significant Z500 or SLP (850 hPa wind) anomalies at the 90% confidence level. Contour intervals are 2 and 1 gpm for (a) and (b), and 0.15 hPa for both (c) and (d). Zero contours are omitted. Units of scale arrows for (c) and (d): m s^{-1}. The solid box in (a) denotes the SC region.

tropical sites. From the SLP and 850 hPa wind regression maps, there is a broad-scale SLP negative anomaly over the Indian Ocean with alongshore cyclonic wind off Sumatra and the Somali coast (see Fig. 2c). Such a circulation feature might reflect the influence of Indian Ocean dipole activity on SC rainfall in boreal summer (Guan and Yamagata, 2003). Finally, there appears to be a wave train in the 500 hPa height field from the subtropics extending into northeast Asia/the north Pacific region (see Fig. 2a). On the other hand, we cannot discern any significant signals at more upstream locations over continental Eurasia.

In the model environment, an analogous relationship between the large-scale circulation and SC rainfall is also found. The Z500 regression map for the MME average shows that increased SC rainfall is associated with a stronger WNPSH over the far WNP to the SCS, with correlation even stronger than that in observations (see Fig. 2b). Interestingly, the MME produces very strong correlation between SC rainfall and Z500 in the tropics; this could be related to the multi-ensemble and multi-model averaging process, which tends to increase the signal-to-noise ratio in the dataset. There is also anomalous anticyclonic flow at 850 hPa and positive SLP in the vicinity and to its east, again bearing much semblance to observations (Fig. 2d). Inspection of the hindcasts from individual models revealed that such a WNPSH (or low-level anticyclone)–SC rainfall relationship is reproduced by models including CWB AGCM, GDAPS, MSC-GM2, NCEP CFS, PNU CGCM and POAMA (figures not shown). In addition, low-level easterly and northeasterly wind perturbations are seen over India and the Arabian Sea to Somalia, respectively. Related to this is a broad-scale positive SLP anomaly spanning the Indian subcontinent to Saudi Arabia. This suggests that the ISM tends to be weaker (stronger) when the SC mean rainfall is enhanced (suppressed) in the MME average. A positive meridional SLP gradient in the northern Indian Ocean is also found in the environments of the CWB AGCM, GDAPS, NCEP CFS, PNU CGCM and POAMA models when they produce above-normal SC rainfall (figures not shown). Finally, there are significant circulation signals over the North Pacific in the MME mean regression map, which are even more robust than their observational counterparts.

We next compared the year-to-year SC rainfall variation from observations and the MME mean of hindcasts. The observed and MME mean rainfall averaged over SC in June, normalized by their respective standard deviations, are given in Fig. 3. The two time series were found to be highly correlated, with a correlation coefficient of 0.73. In other words, the MME average is capable of capturing the SC rainfall variation in June. For individual models, the correlation between their predicted SC rainfall and observations ranged from -0.49 to 0.67. For models that yielded a correlation coefficient of 0.3 or above, most of them (CWB AGCM, GDAPS, NCEP CFS, PNU CGCM and POAMA) reproduced the aforementioned anomalous WNPSH and SLP gradient over the Indian subcontinent associated with SC rainfall changes. This suggests that successfully capturing the WNPSH and ISM–SC regional climate linkages could be important for predicting SC precipitation.

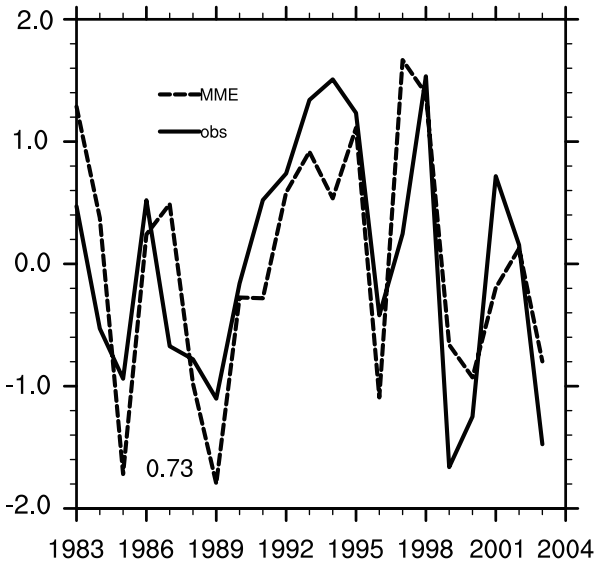

Fig. 3. Standardized SC mean rainfall anomalies in June from observations (solid line) and MME average (dashed line). Correlation between the time series is given in the lower right corner.

3.2. *Station-scale prediction based on direct model outputs and statistical downscaling*

In order to assess the performance of direct model outputs (DMO) in capturing the station-scale rainfall, hindcast precipitation data were first spatially interpolated onto 97 station locations. Temporal correlation between the observed and DMO-derived station-scale rainfall was then computed. The results are shown in Fig. 4. It can be seen that GCPS and NCEP CFS are the most skillful in reproducing the SC rainfall, with correlation reaching 0.6 or more at some stations. On the other hand, for BCC CGCM and MSC_SEF, there are only a few stations with correlation coefficients greater than 0.2. The June rainfall variation in eastern SC seems to be relatively well captured by GCPS, MSC-GM3, NIMR AGCM, and POAMA, whereas CWB AGCM, GDAPS, NCEP CFS and PNU CGCM are more skillful in southern coastal locations. Overall, in the more in-land western to northwestern part of SC, the abilities of the models tend to be lower. Finally, the correlation between the observed and MME mean DMO precipitation at station locations was also computed. Compared to individual models, the MME average gives the best overall performance in predicting the SC station rainfall (as evidenced by the MME mean giving the most number of stations with correlation larger than 0.2; see Fig. 4l). The MME method can reduce forecast uncertainties by better sampling of errors in the circulation–precipitation relations in different models. Thus, in this study, we have been able to demonstrate that even simple averaging of model products can lead to an overall improvement in SC rainfall prediction.

It is evident that DMO prediction can be skillful at some stations in SC, but for other stations realistic forecasts could

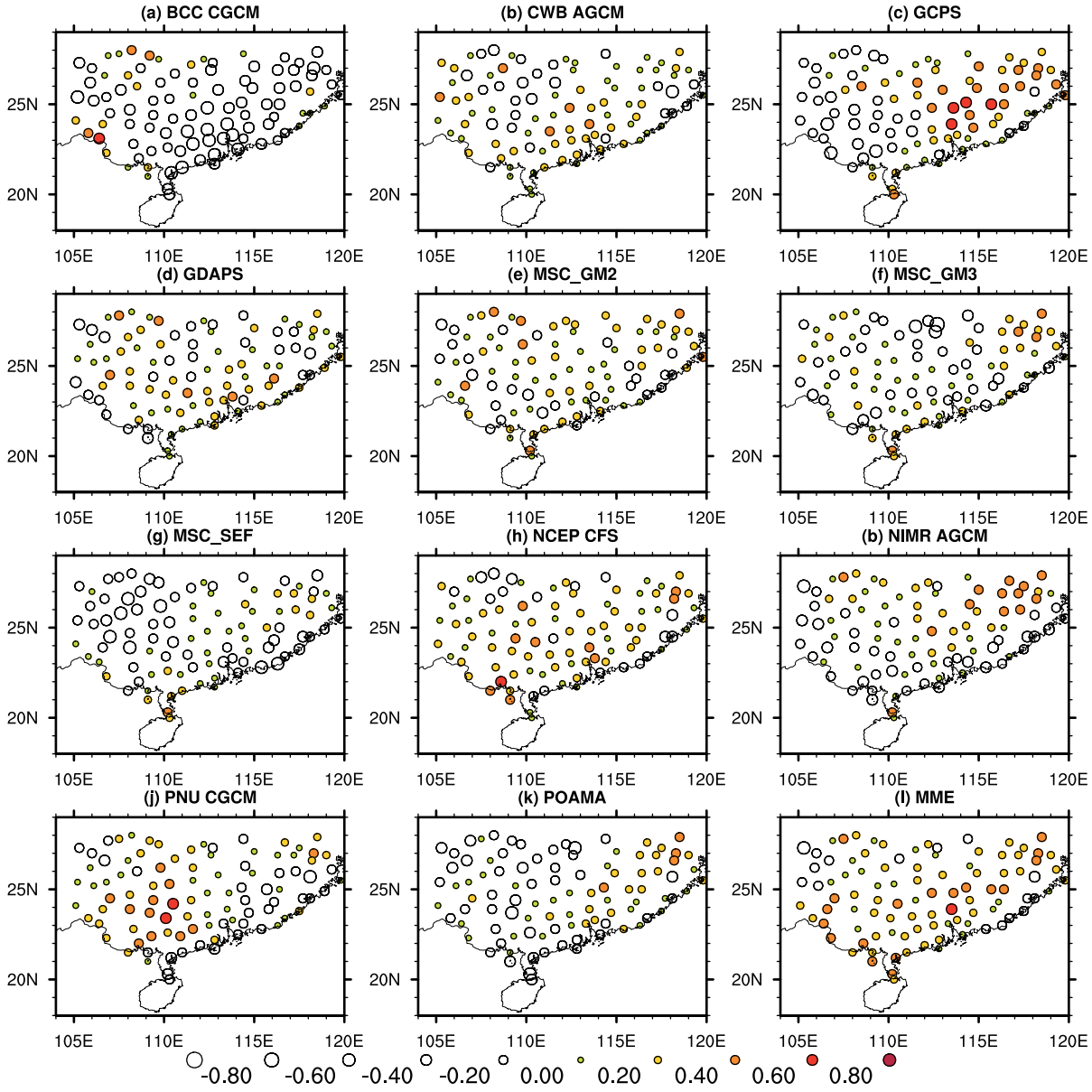

Fig. 4. Correlation coefficients between observed and model-predicted rainfall for June at station locations from (a) BCC CGCM, (b) CWB AGCM, (c) GCPS, (d) GDAPS, (e) MSC-GM2, (f) MSC-GM3, (g) MSC-SEF, (h) NCEP, (i) NIMR AGCM, (j) PNU CGCM, (k) POAMA, and (l) the MME average.

not be achieved. We applied the statistical downscaling technique for the purpose of improving station rainfall prediction by individual models. As shown previously, SC rainfall in June is closely related to WNPSH activity, as well as SLP variations over the ISM region (see section 3.1). We have also seen that such linkages are also reproduced in the model environment. Z500 and SLP simulations over the WNP and Indian Ocean/Indian subcontinent regions, respectively, were therefore chosen as predictors for statistical downscaling. Notice that the regions over which the Z500 and SLP variables are averaged can differ from model to model (see section 2.2 for details of the downscaling method). The exact domains used for spatial averaging are provided in Table 2.

Figure 5 shows the difference between statistical predic-

Table 2. Domains over which the model-predicted SLP and Z500 were averaged for statistical downscaling. See text for details.

Model	Domain A (SLP)	Domain B (Z500)
BCC CGCM	(0°–30°N, 50°–90°E)	(10°–25°N, 130°–180°E)
CWB AGCM	(25°N–10°S, 70°–110°E)	(10°–25°N, 130°–180°E)
GCPS	(15°N–10°S, 50°–90°E)	(5°–20°N, 130°–180°E)
GDAPS	(15°N–10°S, 50°–90°E)	(0°–20°N, 130°–180°E)
MSC_GM2	(15°N–10°S, 70°–90°E)	(10°–20°N, 130°–180°E)
MSC_GM3	(25°N–10°S, 50°–110°E)	(15°–30°N, 130°–180°E)
MSC_SEF	(25°N–10°S, 60°–120°E)	(10°–25°N, 130°–180°E)
NCEP CFS	(25°N–10°S, 60°–130°E)	(10°–25°N, 120°–180°E)
NIMR AGCM	(10°N–10°S, 50°–130°E)	(10°–25°N, 120°–160°E)
PNU CGCM	(10°N–10°S, 60°–110°E)	(10°–30°N, 120°–180°E)
POAMA	(5°–30°N, 90°–140°E)	(0°–25°N, 130°–180°E)
MME	(20°N–10°S, 60°–110°E)	(5°–25°N, 130°–180°E)

tion–observation correlation and DMO–observation correlation, for each individual model as well as their MME mean. There are 50 stations over which the downscaling scheme can improve the rainfall perdition for BCC CGCM, with improvement of the correlation by greater than 0.6 at some locations. Most of these stations are found in southern locations of SC near the Pearl River Delta and to its west in Guangdong (solid circles in Fig. 5a), where the correlation between observations and DMO is about -0.2 to -0.3. The number of stations in SC at which statistical downscaling outperforms DMO in predicting the June rainfall is also provided in Fig. 6. For GDAPS, MSC_GM2 and the MME average, the statistical scheme is able to improve the rainfall prediction only at a handful of stations. It can be seen that downscaling can improve predictions where the DMO performance is poor (see Fig. 4 for the skill of DMO). Statistical downscaling leads to improvement at about 30 stations for NCEP, many of them located in southeastern coastal SC (see Fig. 5h). Statistically downscaled rainfall prediction outperforms DMO for NIMR AGCM at more than 40 stations, which are located mainly in the southern part of the domain (see Fig. 5i).

To further examine why downscaling can greatly improve the skill of the two models, large-scale circulation variables were regressed onto the observed June rainfall averaged over those locations with prediction improvements. It was found that above-normal precipitation over the Pearl River Delta (corresponding to stations where downscaling leads to improvement for BCC CGCM; see Fig. 5a) is positively cor-

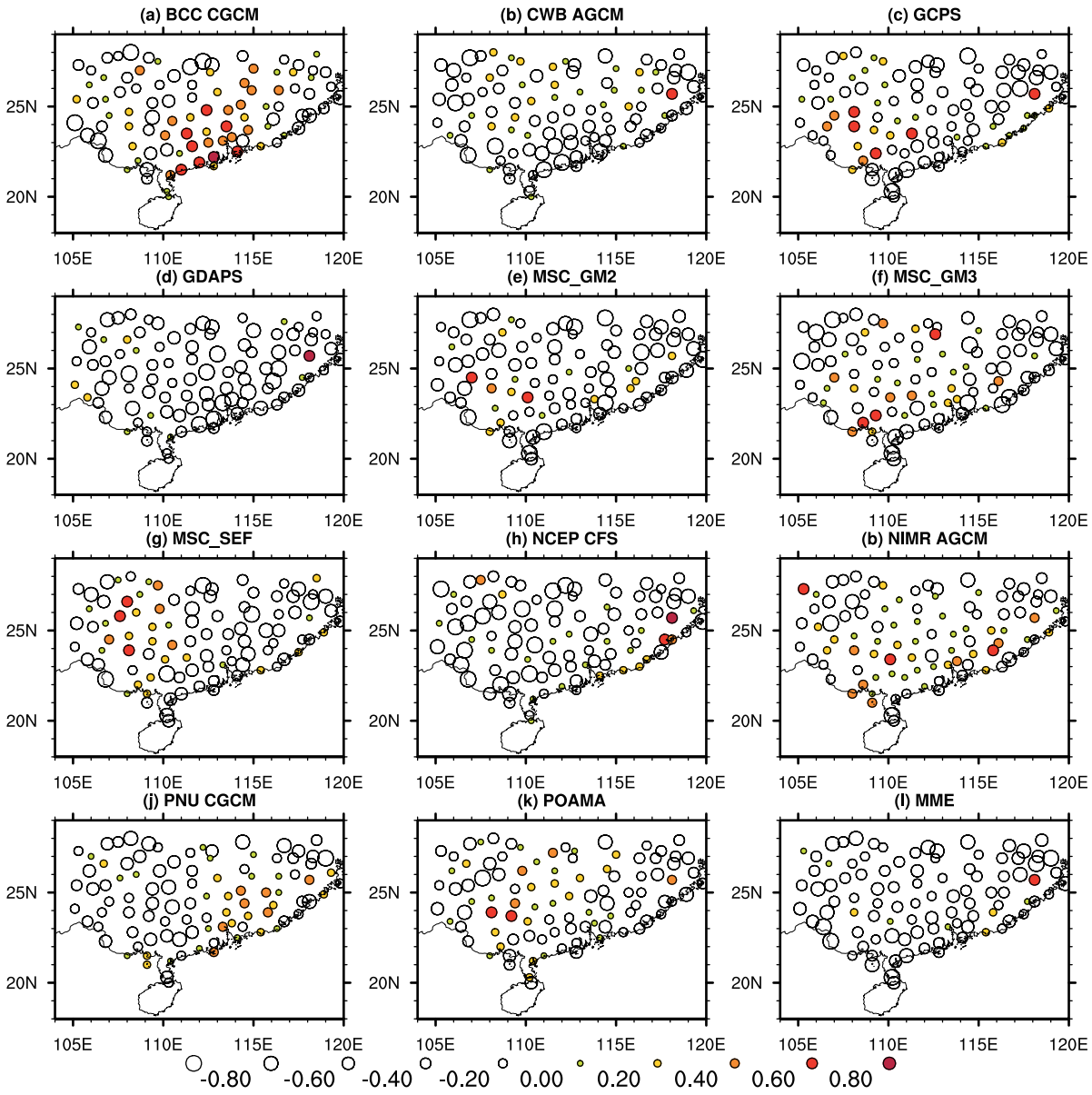

Fig. 5. Correlation coefficient difference between direct model predictions and statistical downscaling predictions for (a) BCC CGCM, (b) CWB AGCM, (c) GCPS, (d) GDAPS, (e) MSC-GM2, (f) MSC-GM3, (g) MSC-SEF, (h) NCEP, (i) NIMR AGCM, (j) PNU CGCM, (k) POAMA, and (l) the MME average.

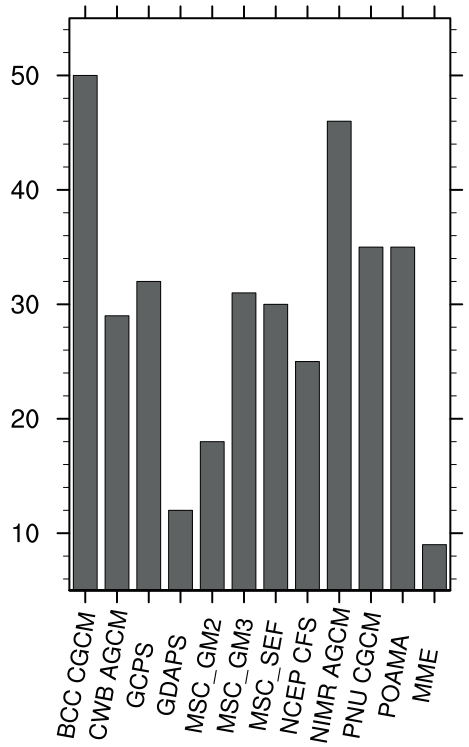

Fig. 6. Number of stations over which statistical downscaling prediction outperforms the direct model rainfall prediction for June.

related with BCC CGCM SLP over the Indian Ocean/Indian subcontinent region (figures not shown). An analogous relationship was also found between the observed meridional SLP gradient over the Indian Ocean/Indian subcontinent region and the rainfall variations over the SC (see section 3.1). On the other hand, the regression map for BCC CGCM shows a positive SLP anomaly over the Indian sub-continent right in domain A (i.e. the region over which model SLP values were used for statistical downscaling; see Table 2). Thus, there is an inverse relationship between observed rainfall at these select stations and the strength of the ISM in the BCC CGCM model. Such a relation is exploited by the station-based statistical downscaling scheme for local SC precipitation prediction, leading to improvements in June rainfall prediction. As for the NIMR AGCM, anomalous Z500 in the SCS extending into the WNP is linked to the observed rainfall variations in the corresponding station locations (figures not shown). Apparently, the station-based statistical downscaling scheme can make use of such a linkage to successfully enhance the prediction skill over these selected stations.

4. Discussion and summary

The performance of 11 dynamical seasonal prediction systems as well as their MME mean in predicting the June SC rainfall was assessed. It was found that the MME mean is skillful in capturing the rainfall variation averaged over the SC domain. The relationship between SC rainfall and the atmospheric large-scale circulation over the Indo-Pacific region in the reanalysis data and model environment was also examined. Observations showed that enhanced rainfall over SC is accompanied by stronger WNPSH activity and possibly weaker ISM in June. Such SC rainfall–WNPSH and ISM linkages were also seen in the MME mean as well as the hindcast runs from a number of models. The MME mean (and some of the individual models) might benefit from this and therefore show good skill in forecasting the June SC rainfall.

The performances of individual models and the MME in terms of their June rainfall predictions at 97 SC stations were also assessed. Overall, the MME mean also outperforms all individual models in capturing the station SC rainfall variability. The better performance of the MME average may be related to the better sampling of model uncertainties in the MME method. Some models (e.g. NCEP CFS and GCPS) are also considerably more skillful than others in their station-scale rainfall predictions. On the other hand, most individual models and the MME mean demonstrate very little skill at some locations, such as in-land western SC and eastern coastal SC. Finally, a few individual models such as BCC CGCM and MSC_SEF possess almost no ability to predict rainfall at many stations in SC.

We also carried out station-based statistical downscaling, in an attempt to improve station rainfall prediction. Model circulation patterns were directly linked to the observed station rainfall in a statistical scheme, enabling climate signals from the simulated large-scale circulation to be utilized for station-scale prediction. In particular, SLP and Z500 averaged over the ISM and WNP regions, respectively, were chosen as predictors for downscaling prediction. Cross-validated prediction results were then compared to those based on DMO. It was found that statistical downscaling can lead to more skillful forecasts compared to DMO at more than 30 station locations for seven models (out of a total of 12 hindcast runs, including the MME mean). Improvements brought about by statistical downscaling for BCC CGCM and NIMR AGCM were particularly noticeable. Further inspection of their simulations revealed that rainfall variations at some SC locations were robustly linked to the Indo-Pacific circulation changes in these two models. In addition, we also compared the performance of DMO and statistical downscaling for selected years. For June 1999, the statistical scheme can even outperform DMO in five different models regionally, to such an extent that the scheme can correct a bias in the MME over the southern coast of SC. Overall, the statistical scheme can apparently tap into the abilities of models to capture the large-scale circulation, thereby providing reasonably skillful station-scale rainfall predictions for these models.

To summarize, a number of dynamical models examined in this study, and especially the MME mean, can successfully predict the June rainfall averaged over SC. The MME average also gives reasonably accurate predictions at the station scale, except for some locations in SC. The performance of individual models in capturing station-scale rainfall is much more variable, but the skill of some models can be improved by employing statistical downscaling. Reliable predictions of

the hydrological variations in this region would be useful for the water management sector, as well as for disaster mitigation and adaptation. The approaches to making such predictions highlighted in the present study could prove useful in these respects.

Acknowledgements. The authors thank those institutes participating in the APCC multi-model ensemble operational system for providing the hindcast experiment data. This study was supported by the City University of Hong Kong (Grant No. 9360126).

REFERENCES

Back, S. K., J. H. Ryu, and S. B. Ryoo, 2002: Analysis of the CO_2 doubling experiment using METRI AGCM Part I: The characteristics of regional and seasonal climate response. *J. Korean Meteor. Soc*., **38**, 465–477.

Chang, C. P., and G. T. J. Chen, 1995: Tropical circulations associated with southwest monsoon onset and westerly surges over the South China Sea. *Mon. Wea. Rev.*, **123**, 3254–3267.

Chang, C.-P., Y. Zhang, and T. Li, 2000: Interannual and interdecadal variations of the East Asian summer monsoon and tropical Pacific SSTs. Part II: Meridional structure of the monsoon. *J. Climate*, **13**, 4326–4340.

Chowdary, J., S. P. Xie, J. Y. Lee, Y. Kosak, and B. Wang, 2010: Predictability of summer Northwest Pacific climate in eleven coupled model hindcasts: Local and remote forcing. *J. Geophys. Res.*, **115**, D22121, doi: 10.1029/2010JD014595.

Ding, Y. H., 2004: Seasonal march of the East Asian summer monsoon. *East Asian Monsoon,* C.-P. Chang, Ed., World Sci., 3–53.

Ding, Y. H., Y. Q. Ni, X. H. Zhang, W. J. Li, M. Dong, Z.-C. Zhao, Z. C. Li, and W. H. Shen, 2000: *Introduction to the Short-term Climate Prediction Model System*. China Meteorological Press, 500 pp. (in Chinese)

Doblas-Reyes, F. J., M. Déqué, and J. P. Piedelievre, 2000: Multi-model spread and probabilistic seasonal forecasts in PROVOST. *Quart. J. Roy. Meteor. Soc.*, **126**, 2069–2087.

Fan, K., H. J. Wang, and Y. J. Choi, 2008: A physically-based statistical forecast model for the middle-lower reaches of the Yangtze River valley summer rainfall. *Chinese Science Bulletin,* **53**, 602–609.

Fan, K., Y. Liu, and H. Chen, 2012: Improving the prediction of the East Asian summer monsoon: New approaches. *Wea. Forecasting*, **27**, 1017–1030, doi: 10.1175/WAF-D-11-00092.1

Gao, H., J. He, H, and H. M. Xu, 2001: *Discussion of Determination of the Date of South China Sea Monsoon Onset*. China Meteorological Press, 1–41. (in Chinese)

Guan, Z. Y., and T. Yamagata, 2003: The unusual summer of 1994 in East Asia: IOD teleconnections. *Geophys. Res. Lett.*, **30**, 1544, doi: 10.1029/2002GL016831.

Huang, R. H., and Y.-F. Wu, 1989: The influence of ENSO on the summer climate change in China and its mechanism. *Adv. Atmos. Sci.*, **6**, 21–32, doi: 10.1007/BF02656915.

Kanamitsu, M., W. Ebisuzaki, J. Woollen, S. K. Yang, J. J. Hnilo, M. Fiorino, and G. L. Poter, 2002: NCEP-DOE AMIP-II reanalysis (R-2). *Bull. Amer. Meteor. Soc.*, **83**, 1631–1643.

Kang, H. W., K.-H. An, C.-K. Park, A. L. S. Solis, and K. Stitthichivapak, 2007: Multimodel output statistical downscaling prediction of precipitation in the Philippines and Thailand. *Geophys. Res. Lett.*, **34**, L15710, doi: 10.1029/2007GL030730.

Kang, I.-S., J.-Y. Lee, and C.-K. Park, 2004: Potential predictability of summer mean precipitation in a dynamical seasonal prediction system with systematic error correction. *J. Climate*, **17**, 834–844.

Karl, T. R., W. C. Wang, M. E. Schlesinger, R. W. Knight, and D. Portman, 1990: A method of relating general circulation model simulated climate to the observed local climate. Part I. Seasonal statistics. *J. Climate*, **3**, 1053–1079, doi: http://dx.doi.org/10.1175/1520-0442(1990)003<1053:AMORGC>2.0.CO;2.

Kripalani, R. H., and A. Kulkarni, 2001: Monsoon rainfall variations and teleconnections over South and East Asia. *Int. J. Climatol.*, **21**, 603–616.

Krishnamurti, T. N., C. M. Kishtawal, T. E. LaRow, D. R. Bachiochi, Z. Zhang, C. E. Williford, S. Gadgil, and S. Surendran, 1999: Improved weather and seasonal climate forecasts from multimodel superensemble. *Science*, **285**, 1548–1550.

Krishnamurti, T. N., C. M. Kishtawal, D. W. Shin, and C. E. Williford, 2000: Multimodel superensemble forecasts for weather and seasonal climate. *J. Climate*, **13**, 4196–4216.

Kug, J. S., J. Y. Lee, I. S. Kang, B. Wang, and C. K. Park, 2008: Optimal multi-model ensemble method in seasonal climate prediction. *Asia–Pac. J. Atmos. Sci.*, **44**, 259–267.

Lee, J.-Y., and Coauthors, 2010: How are seasonal prediction skills related to models' performance on mean state and annual cycle? *Climate Dyn.*, **35**, 267–283, doi: 10.1007/s00382-010-0857-4.

Lee, J.-Y., B. Wang, Q. Ding, K. J. Ha, J. B. Ahn, A. Kumar, B. Stern, and O. Alves, 2011a: How predictable is the Northern Hemisphere summer upper-tropospheric circulation? *Climate Dyn.*, **37**, 1189–1203, doi: 10.1007/s00382-010-0909-9.

Lee, S. S., J. Y. Lee, K. J. Ha, B. Wang, and J. K. E. Schemm, 2011b: Deficiencies and possibilities for long-lead coupled climate prediction of the western North Pacific-East Asian summer monsoon. *Climate Dyn.*, **36**, 1173–1188, doi: 10.1007/s00382-010-0832-0.

Lee, W. J., and Coauthors, 2009: APEC 2009 final report. APEC Clim. Cent., Pusan, South Korea. [Available online at http://www.apcc21.net/en/activities/publications/reports/].

Liang, J. Y., S. Yang, Z. Z. Hu, B. H. Huang, A. Kumar, and Z. Q. Zhang, 2009: Predictable patterns of the Asian and Indo-Pacific summer precipitation in the NCEP CFS. *Climate Dyn.*, **32**, 989–1001, doi: 10.1007/s00382-008-0420-8.

Liou, C. S., and Coauthors, 1997: The second generation global forecast system at the central weather bureau in Taiwan. *Wea. Forecasting*, **12**, 653–663.

Liu, Y., and K. Fan, 2014: An application of hybrid downscaling model to forecast summer precipitation at stations in China. *Atmos. Res.*, **143**, 17–30, doi: 10.1016/j.atmosres.2014.01.024.

Liu, Y., K. Fan, and H.-J. Wang, 2011: Statistical downscaling prediction of summer precipitation in Southeastern China. *Atmos. Ocean. Sci. Lett.*, **4**, 173–180.

McFarlane, N. A., G. J. Boer, J. P. Blanchet, and M. Lazare, 1992: The Canadian climate centre second generation circulation model and its equilibrium climate. *J. Climate*, **5**, 1013–1044.

Murakami, T., and J. Matsumoto, 1994: Summer monsoon over the Asian continent and the western North Pacific. *J. Meteor. Soc. Japan*, **72**, 719–745.

Palmer, T. N., and Coauthors, 2004: Development of a European

Multimodel Ensemble System for Seasonal-to-Interannual Prediction (DEMETER). *Bull. Amer. Meteor. Soc.*, **85**, 853–872.

Park, H., B. K. Park, D. K. Rha, and J. Y. Cho, 2002: An improvement of global model in 2001. KMA/NWPD Tech. Rep., 2002–1 (in Korean).

Ritchie, H., 1991: Application of the semi-Lagrangian method to a multilevel spectral primitive-equations model. *Quart. J. Roy. Meteor. Soc.*, **117**, 91–106.

Saha, S., and Coauthors, 2006: The NCEP climate forecast system. *J. Climate*, **19**, 3483–3517.

Scinocca, J. F., N. A. Mcfarlane, M. Lazare, J. Li, and D. Plummer, 2008: The CCCma third generation AGCM and its extension into the middle atmosphere. *Atmos. Chem. Phys. Discuss.*, **8**, 7883–7930, doi: 10.5194/acpd-8-7883-2008.

Sohn, S.-J., C.-Y. Tam, and J.-B. Ahn, 2013a: Development of a multimodel-based seasonal prediction system for extreme droughts and floods: A case study for South Korea. *Int. J. Climatol.*, **33**, 793–805, doi: 10.1002/joc.3464.

Sohn, S.-J., J.-B. Ahn, and C.-Y. Tam, 2013b: Six-month lead downscaling prediction of winter to spring drought in South Korea based on multi-model ensemble. *Geophys. Res. Lett.*, **40**, 579–583, doi: 10.1002/GRL.50133.

Stockdale, T. N., D. L. T. Anderson, J. O. S. Alves, and M. A. Balmaseda, 1998: Global seasonal rainfall forecasts using a coupled ocean-atmosphere model. *Nature*, **392**, 370–373.

Sun, J. Q., and J. B. Ahn, 2011: A GCM-based forecasting model for the landfall of tropical cyclones in China. *Adv. Atmos. Sci.*, **28**, 1049–1055, doi: 10.1007/s00376-011-0122-8.

Tong, H. W., J. C. L. Chan, and W. Zhou, 2009: The role of MJO and mid-latitude fronts in the South China Sea summer monsoon onset. *Climate Dyn.*, **33**, 827–841.

Tung, Y. L., C.-Y. Tam, S.-J. Sohn, and J.-L. Chu, 2013: Improving the seasonal forecast for summertime South China rainfall using statistical downscaling. *J. Geophys. Res.*, **118**, 5147–5159, doi: 10.1002/jgrd.50367.

Wang, B., J. Y. Lee, I. S. Kang, J. Shukla, N. H. Saji, and C. K. Park, 2007: Coupled predictability of seasonal tropical precipitation. *CLIVAR Exchanges*, **12**, 17–18.

Wang, B., and Coauthors, 2008: How accurately do coupled climate models predict the leading modes of Asian-Australian monsoon interannual variability? *Climate Dyn.*, **30**, 605–619, doi: 10.1007/s00382-007-0310-5.

Wang, B., and Coauthors, 2009: Advance and prospectus of seasonal prediction: Assessment of the APCC/CliPAS 14-model ensemble retrospective seasonal prediction (1980–2004). *Climate Dyn.*, **33**, 93–117, doi: 10.1007/s00382-008-0460-0.

Wang, H., and K. Fan, 2009: A new scheme for improving the seasonal prediction of summer precipitation anomalies. *Wea. Forecasting*, **24**, 548–554, doi: 10.1175/2008WAF2222171.1.

Wigley, T. M. L., P. D. Jones, K. R. Briffa, and G. Smith, 1990: Obtaining sub-grid-scale information from coarse-resolution general circulation model output. *J. Geophys. Res.*, **95**(D2), 1943–1953, doi: 10.1029/JD095iD02p01943.

Wilby, R. L., and T. M. L. Wigley, 1997: Downscaling general circulation model: A review of methods and limitations. *Progress in Physical Geography*, **21**, 530–548.

Wilks, D. S., 1995: *Statistical Methods in the Atmospheric Sciences*. Academic Press, 467 pp.

Wu, R., and B. Wang, 2000: Interannual variability of summer monsoon onset over the Western North Pacific and the underlying processes. *J. Climate*, **13**, 2483–2501.

Xie, S.-P., J. Hafner, H. Tokinaga, Y. Du, T. Sampe, K. M. Hu, and G. Huang, 2009: Indian Ocean capacitor effect on Indo-western Pacific climate during the summer following El Nino. *J. Climate*, **22**, 730–747.

Yang, H., and S. Sun, 2005: The characteristics of longitudinal movement of the subtropical high in the western Pacific in the pre-rainy season in South China. *Adv. Atmos. Sci.*, **22**, 392–400, doi: 10.1007/BF02918752.

Yuan, Y., H. Yang, W. Zhou, and C. Y. Li, 2008: Influences of the Indian Ocean dipole on the Asian summer monsoon in the following year. *Int. J. Climatol.*, **28**, 1849–1859.

Yuan, F., W. Chen, and W. Zhou, 2012: Analysis of the role played by circulation in the persistent precipitation over South China in June 2010. *Adv. Atmos. Sci.*, **29**, 769–781, doi: 10.1007/s00376-012-2018-7.

Zhang, Q. Y., and S. Y. Tao, 1998: Influence of Asian mid-high latitude circulation on East Asian summer rainfall. *Acta Meteorologica Sinica*, **56**, 199–211. (in Chinese).

Zhong, A., H. H. Hendon, and O. Alves, 2005: Indian Ocean variability and its association with ENSO in a global coupled model. *J. Climate*, **18**, 3634–3649.

Zhou, W., J. C. L. Chan, and C. Y. Li, 2005: South China Sea summer monsoon onset in relation to the off-equatorial ITCZ. *Adv. Atmos. Sci.*, **22**, 665–676, doi: 10.1007/BF02918710.

Zhou, W., and J. C. L. Chan, 2007: ENSO and the South China Sea summer monsoon onset. *Int. J. Climatol.*, **27**, 157–167.